

Disentangling Rotational Dynamics and Ordering Transitions in a System of Self-Organizing Protein Nanorods *via* Rotationally Invariant Latent Representations

Sergei V. Kalinin,^{1,1} Shuai Zhang,^{2,3} Mani Valletti,⁴

Harley Pyles,^{5,6} David Baker,^{5,6,7} James J. De Yoreo,^{2,3} and Maxim Ziatdinov^{1,8,2}

¹ Center for Nanophase Materials Sciences, Oak Ridge National Laboratory, Oak Ridge, TN 37831, USA

² Materials Science and Engineering, University of Washington, Seattle, WA 98195, USA

³ Physical Sciences Division, Pacific Northwest National Laboratory, Richland, WA 99354, USA

⁴ Bredesen Center for Interdisciplinary Research, University of Tennessee, Knoxville, TN 37996, USA

⁵ Department of Biochemistry, University of Washington, Seattle, WA 98195, USA

⁶ Institute for Protein Design, University of Washington, Seattle, WA 98195, USA

⁷ Howard Hughes Medical Institute, University of Washington, Seattle, WA 98195, USA

⁸ Computational Sciences and Engineering Division, Oak Ridge National Laboratory, Oak Ridge, TN 37831, USA

Abstract

The dynamic of complex ordering systems with active rotational degrees of freedom exemplified by protein self-assembly is explored using a machine learning workflow that combines deep learning-based semantic segmentation and rotationally invariant variational autoencoder-based analysis of orientation and shape evolution. The latter allows for disentanglement of the particle orientation from other degrees of freedom and compensates for lateral shifts. The disentangled representations in the latent space encode the rich spectrum of local transitions that can now be visualized and explored *via* continuous variables. The time dependence of ensemble averages allows insight into the time dynamics of the system, and in particular, illustrates the presence of the potential ordering transition. Finally, analysis of the latent variables along the single-particle trajectory allows tracing these parameters on a single particle level. The proposed approach is expected to be universally applicable for the description of the imaging data in optical, scanning

¹ sergei2@ornl.gov

² ziatdinovma@ornl.gov

probe, and electron microscopy seeking to understand dynamics of complex systems where rotations are a significant part of the process.

Keywords: *self-assembly, latent space models, deep learning, variational autoencoder, representation learning*

Emergence of ordered patterns in the systems of interacting particles is one of the foundational phenomena in chemistry,¹ condensed matter physics,² materials science,³ and biology, encompassing areas ranging from the formation of atomic lattices, protein complexes, and lipid membranes, to the self-assembly of viruses and nanoparticles.^{2,4-6} Correspondingly, understanding of the evolution of such systems and the mechanisms guiding the emergence of the order have remained on the forefront of physical research for over half a century. This effort includes both the theoretical and simulation analysis,^{7,8} exploring both natural structures, and model systems such as colloidal crystals^{2,9} that allow for tunability of underpinning interactions.^{10,11}

One of the challenges in understanding the dynamics of pattern emergence in these systems is the nature of the descriptors of the systems, *i.e.* the compact representation of the local and global geometries. In the systems with long-range translation symmetry, like crystalline lattices, these can be naturally described in the form of the lattice and primitive unit cells. Deviations from ideal behaviors can be further analyzed in terms of the symmetry breaking phenomena, which yields the concepts of order parameters, *etc.* However, the descriptions are considerably more complex in the absence of long-range translational symmetry, as is the case for liquids and liquid crystals. The local descriptors are often constructed based on corresponding correlation functions and structure factors. The advantage of this approach is that it provides descriptors that can be derived from macroscopic scattering experiments, allowing experimental studies of such systems as a function of global stimuli such as temperature, chemical potentials, external fields, and time.

The rapid emergence of real space imaging methods and corresponding model systems have provided the insight into the mechanisms and dynamics of the self-organization phenomena on the single particle levels. Notable examples include optical microscopy of colloid crystals assembly, scanning probe microscopy of nanoparticle and molecular self-assembly,¹²⁻¹⁴ and environmental electron microscopy of nanoparticle dynamics.^{15,16} As such, observations of system evolution particle-by particle and even the partial or full trajectory reconstructions have become common. The progress in the dynamic scanning transmission electron microscopy enabled these studies even on the atomic level, providing insight into the chemical reactions and phase transformations induced by the electron beam, temperature, and other environmental stimuli.¹⁷⁻²²

However, this proliferation of the modelling and experimental data has brought forth the challenge of associated local descriptors, as a necessary step towards comparing local mechanisms to the theoretical models and scattering studies. For spherical particles interacting through isotropic

or angle-dependent force fields, such local descriptors can be derived from local bonding geometries. Traditionally, these descriptors are based on the coefficients of the spherical functions expansions, giving rise to *e.g.* tetratic and hexatic order parameters.²³⁻²⁵ Recent emergence of the machine learning methods, specifically linear dimensionality reduction methods such as principal component analysis, density based methods such as DBSCAN and UMAP, and manifold learning methods such as Isomap and tSNE have stimulated exploration of these systems using these reduced implementations.²⁶ Similarly, self-organized feature maps and (variational) autoencoders have recently been explored.²⁷ Common for all these methods is the projection of the high-dimensional local descriptors (*e.g.* coordinates of particle neighbors) on the low dimensional manifold, providing the reduced descriptors of local geometry that can further be correlated with functional properties. Recent overview of this field is given by Volpe.²⁸ In the last year, the advances in graph networks have stimulated rapid emergence of graph based methods for structural description.²⁹⁻³¹ Finally, when applied to time-dependent structural data, the machine learning methods have been used to identify collective variables³²⁻³⁴ and reaction pathways.³⁵

However, extension of this approach for the anisotropic particles, *e.g.* rod-like or having more complex geometries, leads to the rapid growth of the number of possible ad-hoc descriptors.^{36, 37} The primary difficulty in this case becomes the presence of multiple rotational variants, leading to entanglement between particle shapes and inter particle geometric parameters such as spacings and interaction geometries. Furthermore, comparison with the experiment becomes progressively more complex. These challenges are obvious even in theory, where the analysis of interaction and structure evolution in systems of non-spherical particles evolved much slower than for spherical ones. These difficulties are progressively magnified for the experimental systems, characterized by the presence of the particle size distributions, noise, *etc.*

Here we introduce the approach for the analysis of the structure evolution in the system of interacting anisotropic particles based on a combination of deep fully convolutional neural networks and variational autoencoders (VAEs) with rotational invariance. This methodology particularly relies on the recognized capability of the VAEs to reduce high-dimensional data sets to the low-dimensional continuous latent variables, and disentangle the representations, *i.e.* discover the significant trends in data.³⁸⁻⁴² The examples of such trends are writing styles in handwritten digit data bases or emotional states in human face databases. Introduction of the rotation angle in the image plane as one of the latent variables allows identification of the variants of the

same shape at multiple orientations. In this manner, we introduce the parsimonious particle level descriptors for the system. The time dynamics of the global averages provide the insight into the system evolution, emergence of order, and phase transitions, whereas trajectory-level analysis yields insight into particle dynamics. Note that while this approach is illustrated here for a specific case of particle self-assembly visualized *via* liquid atomic force microscopy, it is in fact universal and can be applied for the analysis of structure evolutions across broad experimental and theoretical domains.

Results and Discussion

As a model system, we explore the self-assembly of a *de novo* designed helical repeat protein DHR10-mica18 (where 18 indicates the number of repeats of the protein),⁴³ on muscovite mica (*m*-mica) which was recorded by high-speed atomic force microscopy (HS-AFM). Inspired by how antifreeze proteins bind ice crystal surfaces, DHR10-mica18 geometrically matches the potassium (K^+) sublattice on the (001) plane of *m*-mica with a designed interface containing 54 carboxylate residues. Its large size and aspect ratio allows individual proteins to be resolved as they adsorb to the mica surface and assemble into ordered structures that are modulated by the concentration of salt in solution.⁴³ With 100 mM KCl, DHR10-mica18 self-assembles into numerous discrete domains aligned along one of the three closed-packed K^+ lattice-directions. However, the close-packed matrix does not have a steady state, instead the domains fluctuate in both direction and size and hence the relative positions of individual proteins within the domains remain dynamic as well, Figure 1. Tracking DHR-10-mica18 on *m*-mica with *in-situ* HS-AFM generates a large amount of data (hundreds of frames with tens of protein molecules in each frame), that is beyond the capability of manual approaches of statistical analysis to define descriptors of the self-assembly process. Here, we develop a machine learning approach to explore this process.

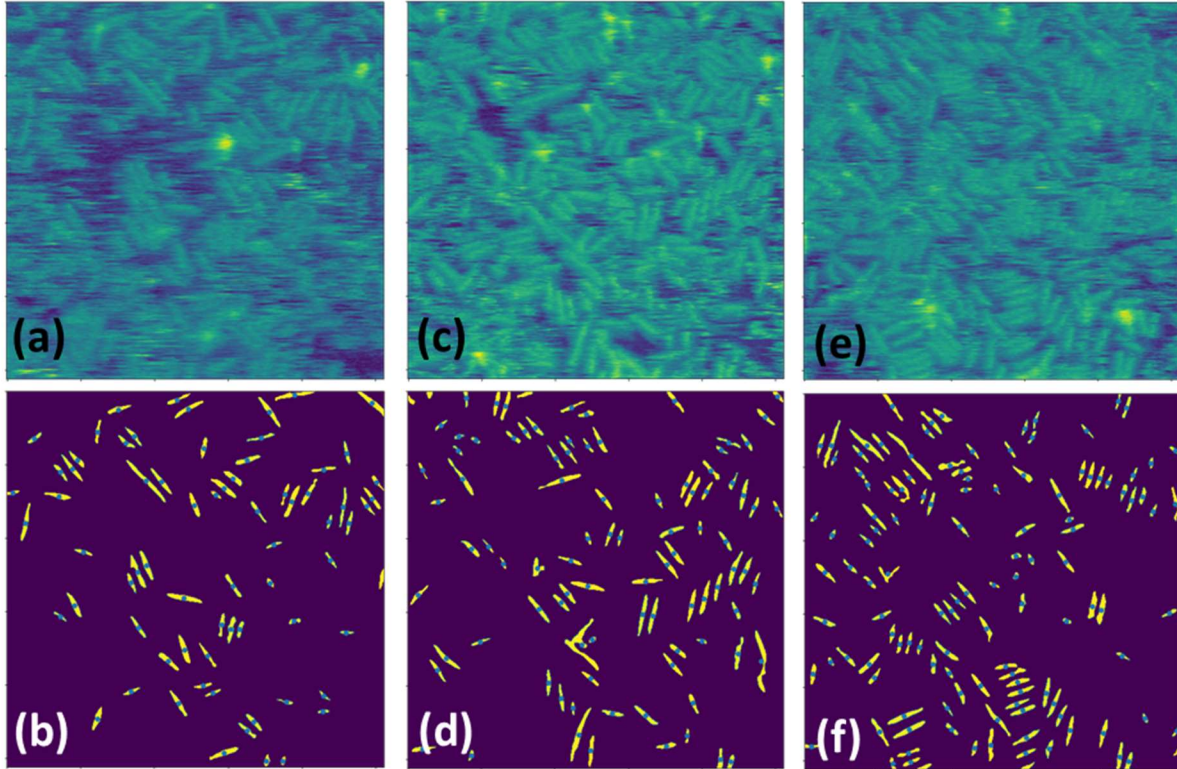


Figure 1. The AFM studies of the dynamics of protein organization. Shown are raw AFM images (top row) and neural network reconstructions (bottom row) for frames (a,b) +131.6 s, (c,d) +263.2 s and (e,f) +394.7 s. The dots in (b,d,f) mark the positions of the centers of gravity of the particles. Image size is 200 nm and frame rate is 0.38 Hz.

To analyze particle positions and orientations visualized in AFM data, we first use the deep convolutional neural network (DCNN) approach to remove noise and identify particles centers of the mass, size, and orientations *via* semantic segmentation (*i.e.*, identifying each pixel in the image as belonging to the particle or substarte). Previously, this approach has been used for analysis of atomically resolved imaging in Scanning Transmission Electron Microscopy^{44, 45} and Scanning Tunneling Microscopy,⁴⁶ Scanning Electron Microscopy,⁴⁷⁻⁵² Transmission Electron Microscopy,^{50, 53-56} Scanning Probe Microscopy,⁵⁷⁻⁵⁹ Optical microscopy,⁶⁰⁻⁶³ and Transmission X-ray microscopy.^{64, 65} Here, a training set for DCNN is made from the sub-set of original images with clearly discernible particles as features and manually labeled categorical images (particle/not particle) as a target. The training set is augmented *via* rotations, Gaussian noise, and horizontal or vertical flips.

Generally, the U-Net⁶⁶ and its various extensions (Dense-U-Net,⁶⁷ U-Net++,⁶⁸ Res-U-Net,⁶⁹ *etc.*) are considered as the go-to DCNN models for semantic segmentation problems. However, we found that these models may not always properly segment particles that form domains (*i.e.*, are located close to each other) in noisy AFM data, which is likely caused by the information loss during the multiple down-sampling/pooling (and corresponding up-sampling/un-pooling) operations. One solution is to reduce the number of blocks in U-Net (and hence, the number of pooling/un-pooling operations), while increasing the depth of the bottleneck layer and replacing the regular convolutions in the bottleneck layer with cascades of dilated convolutions with different dilation rates. The dilated convolutions help maintaining the ability to recognize features at different scales and the computational feasibility. Here, we use the in-house developed *dilnet* neural network architecture with only one max-pooling (and the corresponding un-pooling operation) to preserve the maximum amount of information and two cascades of dilated convolutions with dilation rates of 2, 4, and 6 in the bottleneck layer. To further improve the network’s predictions, we utilize the deep ensemble approach, where multiple networks with different “training trajectories” are trained in parallel and used for prediction. The ensemble mean prediction and the associated variance provide improved recognition/generalization and uncertainty estimates.⁷⁰ Note that thus trained network ensemble yields the semantically segmented images, *i.e.* for each pixel in the raw image Fig. 1 (a,c,e) the decoded image Fig. 1 (b,d,f) yields the “probability” that it belongs to the particle.

With this information in hand, the positions of the center of mass of individual particles can be readily mapped. Previously, we used the ellipsoid fit to find the characteristic particle sizes and rotation angles. Based on these top-down particle level descriptors, the system evolution in terms of relevant distribution functions and their spatial correlations can be analyzed. In certain cases when the same particle can be traced across multiple frames, the evolution of these parameters along the trajectory can be traced. Note that while these characteristics are readily available in the simulation studies, discovery of these in the experimental data represents a considerable challenge and analysis is naturally limited to the objects that can be discerned by the deep learning network and, for trajectories, the displacements of which is sufficiently small to allow for reconstruction. That said, the subsequent discussion and analysis can be equally applied for both decoded experimental and simulation data.

To get insight into particle dynamic and structure evolution during the self-organization process, here we use a rotationally invariant extension⁷¹ of the variational autoencoder (rVAE). Generally, autoencoders (AE) refer to the class of the neural networks that compress the data set to a small number of latent features, and then expand back to original data set. The training aims to minimize information loss between the initial and reconstructed images *via* usual backpropagation. This process tends to select the relevant features in the data set and reject the noise, giving rise to applications for denoising, *etc.* At the same time, the latent features allow for efficient encoding of the original data set.

Variational autoencoders (VAEs) expand on this concept by substituting the bottleneck latent layer by the latent space, from which the variables for decoding are drawn from a prescribed prior distribution. In this manner, VAEs represent a hybrid of the AE approach for creating generalized encoding and decoding functions, and Bayesian priors for feature selection. Since the Bayesian layer is non-differentiable, the training of the VAEs is based on sampling latent vector using the reparameterization trick as shown by Kingma and Welling.^{38, 39} The unique aspect of VAEs is that they tend to structure the latent space in such a way that the decoded data will have clear variations along the latent directions. This behavior, referred to as disentangled representations,^{72, 73} allows for determination of styles of handwriting of fashion, style transfer, *etc.* More generally, VAEs allow projection of high-dimensional and potentially discrete spaces onto low-dimensional differentiable manifold, potentially allowing for mapping equations of motions, enabling Bayesian optimization, *etc.*

Here, we adapt the variational autoencoder to include the rotation and offsets in x - and y -directions as three of the latent variables, in addition to classical latent variables. In this manner, the rotations of the particles in the image plane are separated as one latent variable, and non-idealities in determination of particle center of mass are captured *via* offsets. The remaining latent variables provide the information on particle shape, structure of the nearest neighborhood, *etc.* depending on the size of the sampling window (size of sub-image cropped around each detected particle). The encoder and decoder of rVAE are chosen to be simple fully connected (“dense”) neural networks.

The semantically segmented DCNN output is used to create an input into the rVAE. The use of the raw data led to relatively smooth decoded features that allow for partial orientation mapping only and was not actively pursued. The latent angles (in this specific case) give rise to

clear multimodal distributions corresponding to 6 possible orientations of the particles on the surface, whereas offset distributions are reasonably narrow and sharp. These criteria were used to identify optimal training and sampling window parameters. Here, we have chosen the windows slightly above the particle length (see Fig. 2d-f), to fully capture the particle shape and the lateral interactions but at the same time avoid excessive details that necessitate high dimensionalities of latent space to describe.

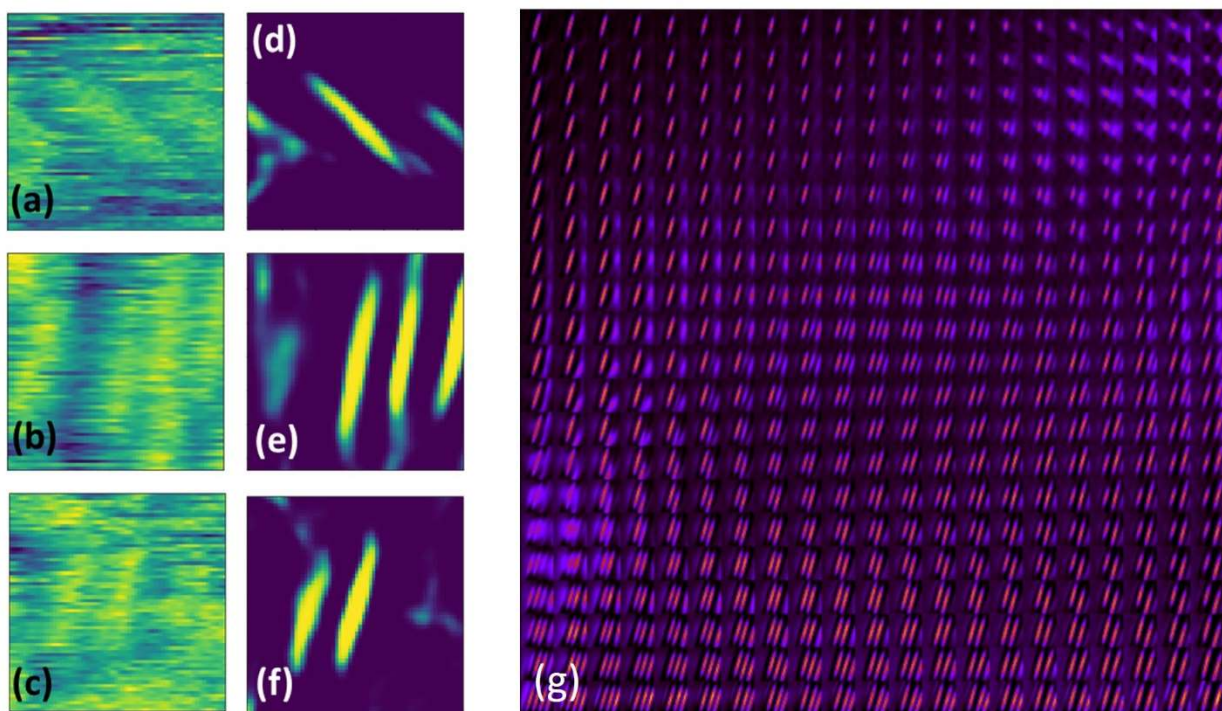


Figure 2. (a,b,c) Several sub-images of the raw data and (d,e,f) corresponding DCNN output. The latter is used for rVAE training. (g) The learned latent space of the rVAE projected onto the image space showing the evolution of the decoded images as a function of latent variables, $d(L_1, L_2)$. The size of sub-images is 25 nm.

The rVAE's training was performed using Adam optimizer⁷⁴ for 3000 epochs with a mini-batch size of 200 for the data set of the $\sim 13,200$ sub-images, as limited by the number of the decoded particles in the data set. The typical sub-images with raw experimental data and corresponding decoded images are shown in Figure 2. rVAE analysis converts each decoded sub-image into the latent angle (L_θ), offsets ($L_{\Delta x}$ and $L_{\Delta y}$), and latent variables associated with

particles structure and spatial arrangement (L_1 and L_2) that now describe the state of each particle. The system behavior can then be analyzed *via* statistical analysis of the time dependence of relevant distributions within each frame as a function of frame number, correlation function analysis, or trajectory analysis.

A convenient way to represent the rVAE operation is through the analysis of latent space representations. The encoding of the sub-images transforms each of the sub-images into 3+2 latent variables. The distribution of the latent variables determines the size of the latent variable space bound by minimal and maximal values of L_1 and L_2 . We can further introduce the uniform rectangular grid of points in the latent space and decode these values to yield the particles geometry. This latent space representation is shown in Fig. 2 (g). Note that the decoded features have a clear physical meaning, representing the single and multiple particles assemblies.

The characteristic aspect of VAEs is their potential for disentangling the data representations, where each latent variable describes the certain trait in data set. This examination of this behavior is visible in Fig. 2 (g), where on transition from left to right (*i.e.*, for constant L_2) the particles become smaller, whereas on vertical the number of particles in decoded sub-image increases. The projected latent space for the vanilla VAE can be found in the Supplemental Material.

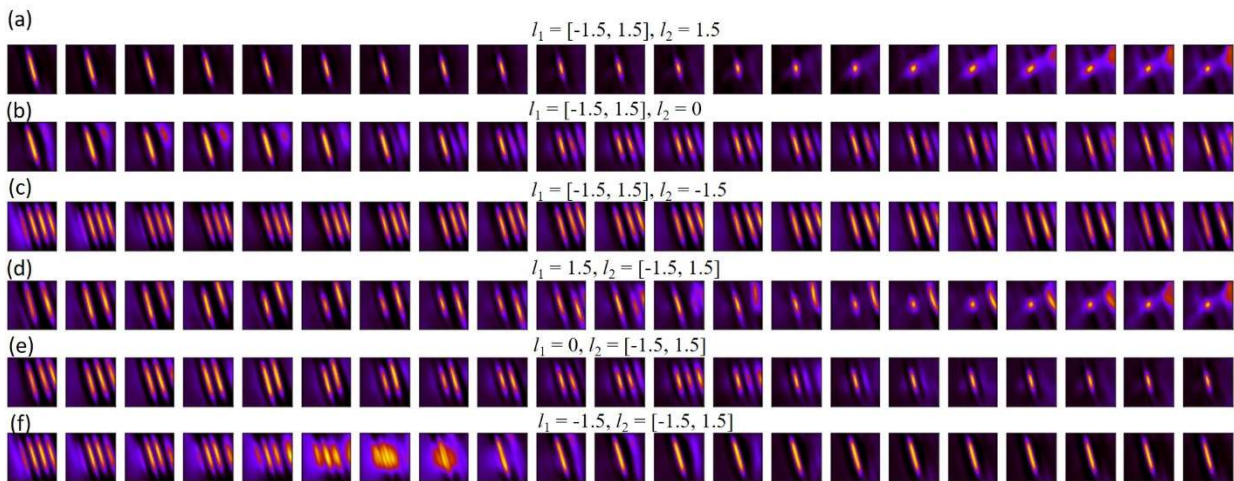


Figure 3. (a,b,c) Magnified cross-sections along the L_1 axis at fixed values of L_2 and (d,e,f) along the L_2 axis along the fixed values of L_1 .

To get further insight into these behaviors, shown in Fig. 3 are the expanded cross-sections from Figure 2 (g) obtained for higher sampling density in latent space. Here, the Fig. 3 (a) shows the gradual evolution of a particle shape, eventually converting to non-physical mixed contrast. Similar variation between physical and unphysical shapes is observed in (d). At the same time, Fig. 3 (b,c,e,f) illustrate the evolution of density of particles across the row.

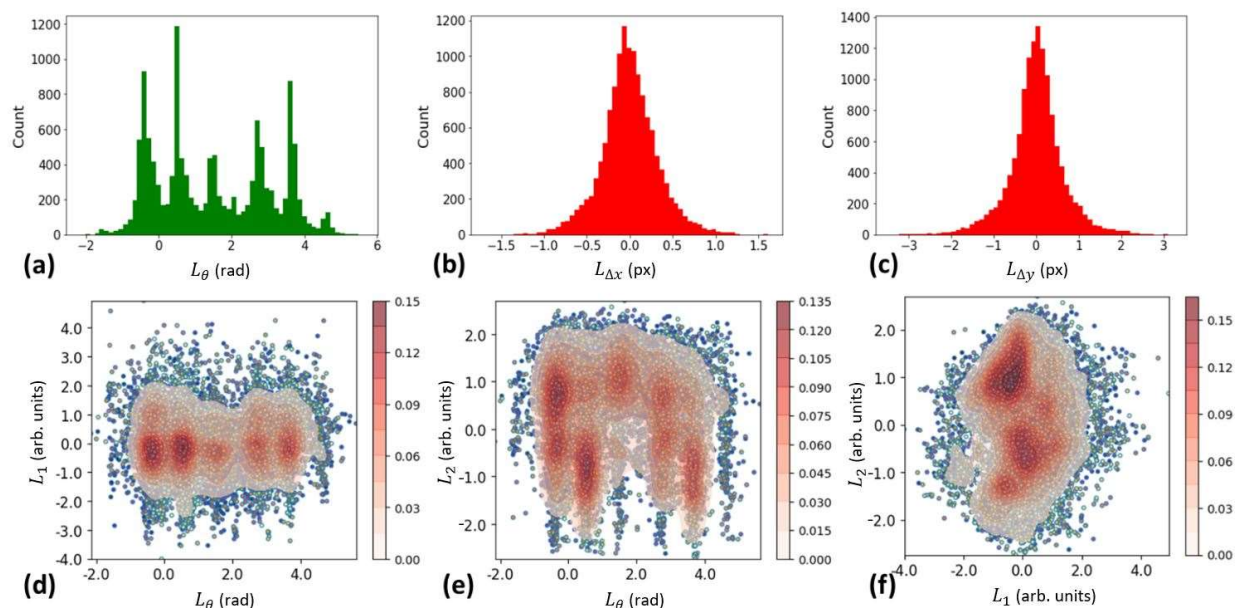


Figure 4. Distributions of latent variables across the full experiment. (a) Distribution of the encoded angle (L_θ) clearly illustrates the presence of six dominant orientations due to the interactions between the nanoparticles and substrate. Note that here particles are not assumed to be symmetric perpendicular to the long axis. (b, c) Distributions of the x - and y -offsets ($L_{\Delta x}$ and $L_{\Delta y}$). These distributions are relatively featureless but indicate the convergence of the rVAE. (d,e,f) Joint distributions between the encoded angle L_θ and latent variables L_1 , L_2 associated with particles structure/arrangement. Shown are the points corresponding to each particle and superimposed is kernel density estimate.

The latent representation analysis allows us to get further insight into the global system dynamics *via* the analysis of the latent parameter distributions and their time dynamics. Shown in Figure 4 is the global (*i.e.* averaged over the full data set) distributions for the latent variables. Here, the angle distributions clearly show 6 peaks, corresponding to preferential orientation of the protein particles due to anisotropic interactions with the substrate. The offset distributions are

relatively featureless and generally confined within one pixel, indicative of successful particle finding (in cases when rVAE fails to converge, much broader distributions are observed). Finally, the joint distributions in latent variable space are shown in Figs. 4 (d-f). Here, we visualize both the individual data points and the superimposed kernel density estimates. Note that the L_1 - L_θ distribution is almost marginalizable, with clear 6-fold maxima associated with angle distribution. At the same time, the L_2 - L_θ distribution is nontrivial, illustrating the presence of the multimodal L_2 distributions for each angle. Comparison with Fig. 2 (g) illustrates that these distributions differ by the lateral spacing between the particles. This behavior is further illustrated in Fig 4 (f), where two primary maxima corresponding to ~ 1 and -1 for L_2 are clearly seen.

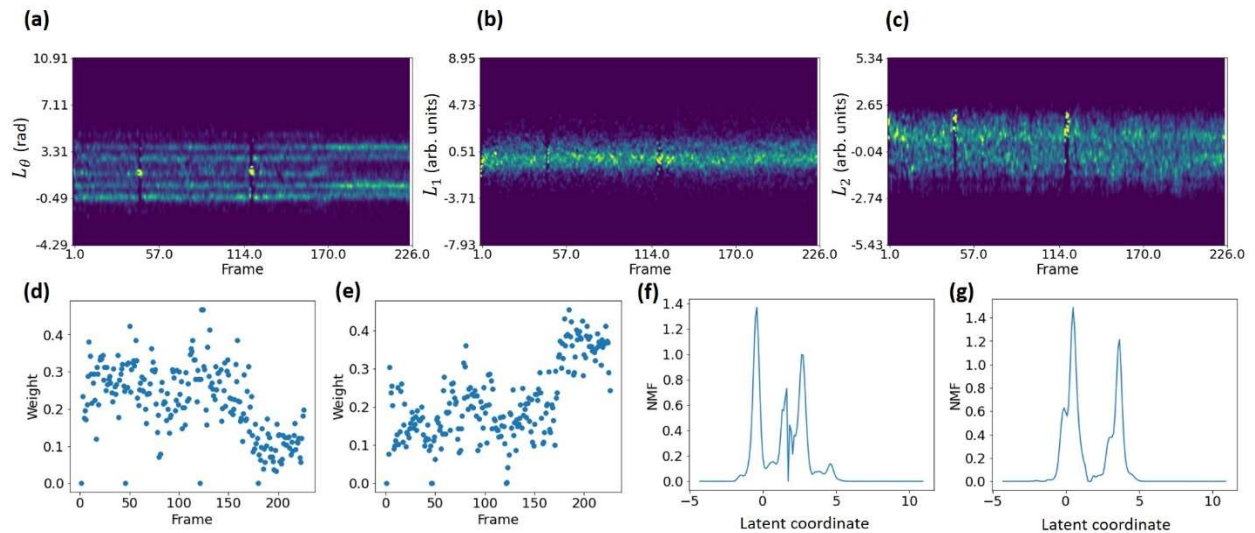


Figure 5. Time dynamics of (a) encoded angle L_θ , (b) first (L_1) and (c) second (L_2) latent variables. (d,e) time dependence of the weights of the first and second NMF component and (f,g) corresponding endmembers. Note that features with lost contrast were excluded from NMF analysis. Clear transitions at frame ~ 170 is visible (a,d).

To get insight into the dynamics of the system, we analyze the time dynamics of the latent variable distribution. To accomplish it, we calculate the 1D kernel density estimates (KDE) for the distribution of the corresponding latent variables, as shown in Fig. 5. The time dynamics of the angle clearly indicates the presence of six rotational variants in the early times, with the transition to only 4 dominant variants on later stages.

The relevant aspects of this behavior can be further analyzed using the suitable dimensionality reduction method. Given that KDE are positively defined, we use the non-negative matrix factorization (NMF) such that a separation of the 2D data set $KDE(L_c, t)$, where L_c is a chosen latent variable and t is time, is represented as

$$KDE(c, t) = \sum_{i=1}^N w_i(L_c) e_i(t) \quad (1)$$

where $w_i(L_c)$ are the NMF weights and $e_i(t)$ are the endmembers that determine characteristic time behaviors. The number of components N is set at the beginning of the analysis and can be chosen based on the quality of decomposition, anticipated physics of the systems, *etc.* Here, after experimentation, the $N = 2$ was found to be sufficient to represent the observed dynamics.

The time dependence of the 1st and 2nd NMF component are shown in Figure 5 (d,e) respectively. Note the sharp change at frame ~ 140 associated with the disappearance of 2 out of 6 orientational variants, *i.e.* spontaneous symmetry lowering in the system.

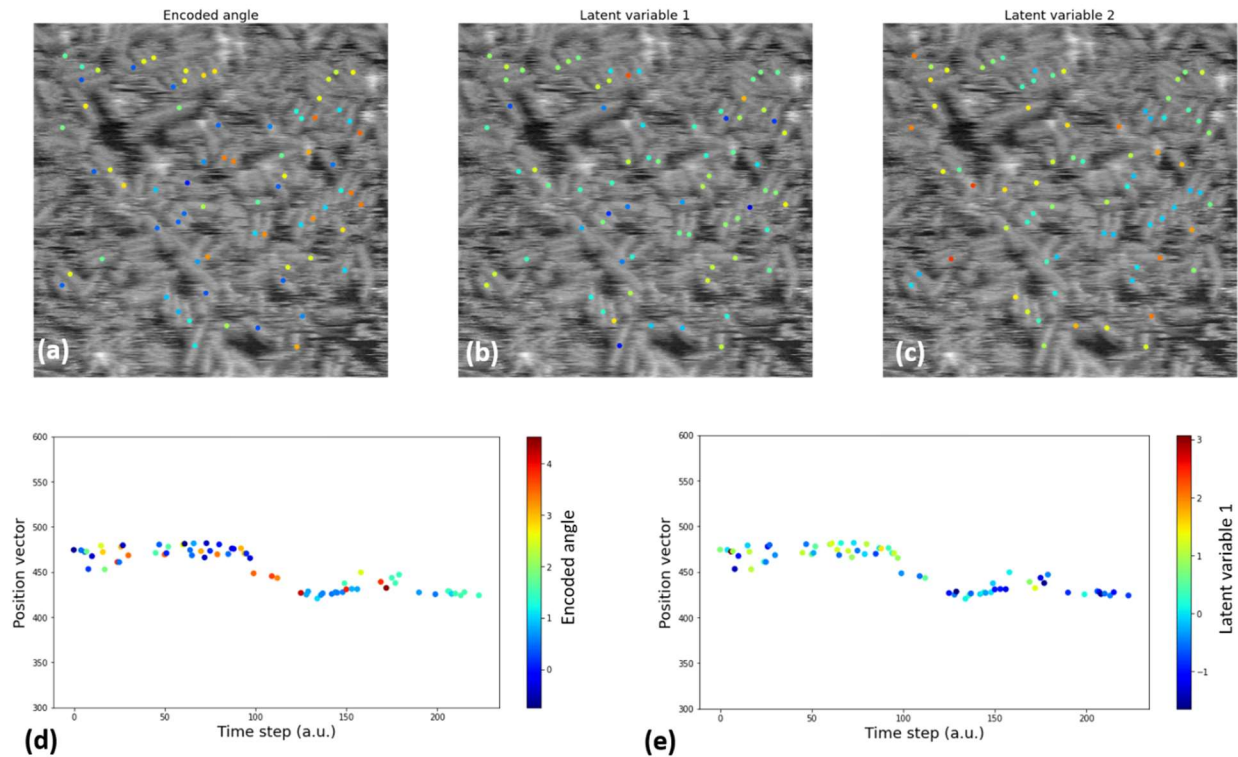


Figure 6. Latent encoding in particle assemblies. (a) Latent angle and (b) first and (c) second latent variables. Note that for ordered phase both parallel (ferroelectric-like) and antiparallel

(antiferroelectric-like) arrangements of the particles can be observed. (d, e) Example of a trajectory of a single particle encoded by angle (d) and the first latent variable (e). Image size is 200 nm.

Finally, the latent representations allow the exploration of the dynamics on a single particle level. Shown in Figure 6 are the raw images at several time steps with the color markers indicative of the corresponding latent variables. In some cases, the particle trajectories can be reconstructed by tracking individual particles from one frame to another *via* the nearest neighbor search. Here the search radius was set to 21 px, which corresponds to 8.2 nm. In this case, the evolution of the latent variable along the trajectory can be explored, as shown in Fig. 6 (d,e). Similarly, the particle dynamics can be explored in the latent space, representing the changes in the particle geometry and nearest neighborhood during the evolution.

Conclusions

To summarize, the particle dynamics during the protein self-assembly was explored using machine learning workflow that combined DCNN based semantic segmentation and rotationally invariant VAE analysis of orientation and shape dynamics. The chosen VAE architecture allows disentangling the particle orientation from other degrees of freedom and compensates for shifts. The disentangled representations in the latent space encode the rich spectrum of local transitions that can now be visualized and explored *via* continuous variables. The time dependence of ensemble averages allows insight into the time dynamics of the system, and in particular illustrates the presence of the potential ordering transition. Finally, analysis of the latent variables along the single particle trajectory allows mapping evolution of particle shape and nearest environment. This approach allowed us to detect the symmetry lowering transitions associated with emergence of long-range order within the structures. More generally, this approach now allows for straightforward analysis of distributions and fluctuations of ordered domains, tied to relative free energies of the various states.

The proposed approach is expected to be universally applicable for the description of the imaging data in optical, scanning probe, and electron microscopy seeking to understand dynamics of complex systems where rotations is a significant part of the process. We note that while here both the DCNN and rVAE were applied to a single class, it can be expanded to multiclass features in a straightforward way. Furthermore, this approach can be used for exploration of

computationally generated datasets, including the evolution of the electronic density and lattice displacements desiring diffusion and reactions in atomistic modelling, dynamics of macromolecules, *etc.* Finally, it directly allows to enumerate and explore transformation mechanisms in system with complex interacting objects *via* analysis of corresponding latent representations.

Methods:

Particle synthesis

DHR10-mica18 proteins were expressed in *E. coli*, purified with nickel NTA affinity and size exclusion chromatography, and dialyzed into 20mM Tris buffer (pH=8). For more details see reference [43].

High-speed atomic force microscopy

DHR10-mica18 protein stock solution was diluted to 0.025 μM with 20 mM Tris buffer (pH=7) having 100 mM KCl. 20 μl diluted protein solution was dropped onto freshly cleaved muscovite-mica (001) (SPI Supplies) and characterized by Cypher Video-Rate AFM (Asylum Research) in liquid amplitude-modulation mode. The probe USC-F1.2-K0.15 (NanoWorld) was used. The imaging force was adjusted to minimize any interruption. Tris-HCl buffer (pH 7, 1 M), and KCl were bought from Sigma-Aldrich. Nuclease-free water was bought from Ambion.

Data analysis

The DCNN and rVAE were implemented *via* AtomAI package.⁷⁵ To train a deep DCNN ensemble we first trained a baseline model for N epochs until test loss reached a plateau. We then trained 12 individual ensemble models for n epoch ($n \ll N$) starting each time with the weights of the baseline model and performing training data shuffling with different random seed. The Adam optimizer⁷⁴ with a learning rate of 0.001 was used for optimizing weights of all the ensemble models. The encoder and decoder of rVAE were 2-layer perceptrons with 128 neurons in each layer activated by $\tanh()$ function whose weights were optimized using Adam optimizer with a learning rate of 0.0001. We have experimented both with the convolutional and fully-connected in the rVAE's encoder and decoder, and for this data did not see significant difference in performance. The latent

space consisted of 5 neurons: one neuron designated to absorb particles rotation, two other neurons designated to absorb particles translation, and the remaining two neurons for capturing the remaining factors of variations (*i.e.*, particles structure). We note that while more neurons can be in principle added to analyze variations in particles structure, it complicates the visualization of the learned latent manifold and has not shown to lead to any additional new insights on this data set.

Supporting Information

The supporting information is available free of charge on the ACS Publication website at DOI: xxxx.

Supplementary figure showing the learned latent manifold of a regular VAE model

Acknowledgment

This research including AFM (S.Z., J.J.D.), data analytics (S.V.K.) and protein design and synthesis (H.P., D.B.) are supported by the US Department of Energy, Office of Science, Office of Basic Energy Sciences, as part of the Energy Frontier Research Centers program: CSSAS–The Center for the Science of Synthesis Across Scales–under Award Number DE-SC0019288, located at University of Washington. The machine learning was performed and partially supported (M.Z.) at the Oak Ridge National Laboratory’s Center for Nanophase Materials Sciences (CNMS), a U.S. Department of Energy, Office of Science User Facility. High-speed AFM experiments were performed at the Department of Energy's Pacific Northwest National Laboratory (PNNL). PNNL is a multi-program national laboratory operated for Department of Energy by Battelle under Contract No. DE-AC05-76RL01830.

References

1. Sharma, V.; Park, K.; Srinivasarao, M., Colloidal Dispersion of Gold Nanorods: Historical Background, Optical Properties, Seed-Mediated Synthesis, Shape Separation and Self-Assembly. *Mater. Sci. Eng. R-Rep.* **2009**, *65* (1-3), 1-38. doi:10.1016/j.mser.2009.02.002
2. Boles, M. A.; Engel, M.; Talapin, D. V., Self-Assembly of Colloidal Nanocrystals: From Intricate Structures to Functional Materials. *Chemical Reviews* **2016**, *116* (18), 11220-11289. doi:10.1021/acs.chemrev.6b00196
3. Wang, T.; Zhuang, J. Q.; Lynch, J.; Chen, O.; Wang, Z. L.; Wang, X. R.; LaMontagne, D.; Wu, H. M.; Wang, Z. W.; Cao, Y. C., Self-Assembled Colloidal Superparticles from Nanorods. *Science* **2012**, *338* (6105), 358-363. doi:10.1126/science.1224221
4. He, J. B.; Niu, Z. W.; Tangirala, R.; Wan, J. Y.; Wei, X. Y.; Kaur, G.; Wang, Q.; Jutz, G.; Boker, A.; Lee, B.; Pingali, S. V.; Thiyagarajan, P.; Emrick, T.; Russell, T. P., Self-Assembly of Tobacco Mosaic Virus at Oil/Water Interfaces. *Langmuir* **2009**, *25* (9), 4979-4987. doi:10.1021/la803533n
5. Marsh, J. A.; Teichmann, S. A., Structure, Dynamics, Assembly, and Evolution of Protein Complexes. *Annual Review of Biochemistry* **2015**, *84* (1), 551-575. doi:10.1146/annurev-biochem-060614-034142
6. Luo, Q.; Hou, C.; Bai, Y.; Wang, R.; Liu, J., Protein Assembly: Versatile Approaches to Construct Highly Ordered Nanostructures. *Chem. Rev.* **2016**, *116* (22), 13571-13632. doi:10.1021/acs.chemrev.6b00228
7. Baule, A.; Mari, R.; Bo, L.; Portal, L.; Makse, H. A., Mean-Field Theory of Random Close Packings of Axisymmetric Particles. *Nature Communications* **2013**, *4*, 11. doi:10.1038/ncomms3194
8. Mahynski, N. A.; Pretti, E.; Shen, V. K.; Mittal, J., Using Symmetry to Elucidate the Importance of Stoichiometry in Colloidal Crystal Assembly. *Nature Communications* **2019**, *10*, 11. doi:10.1038/s41467-019-10031-4
9. Li, B.; Zhou, D.; Han, Y. L., Assembly and Phase Transitions of Colloidal Crystals. *Nature Reviews Materials* **2016**, *1*, 15011. doi:10.1038/natrevmats.2015.11
- 10.1038/natrevmats.2015.11
10. Whitelam, S., Control of Pathways and Yields of Protein Crystallization through the Interplay of Nonspecific and Specific Attractions. *Physical Review Letters* **2010**, *105* (8), 088102. doi:10.1103/PhysRevLett.105.088102
11. Mannige, R. V.; Haxton, T. K.; Proulx, C.; Robertson, E. J.; Battigelli, A.; Butterfoss, G. L.; Zuckermann, R. N.; Whitelam, S., Peptoid Nanosheets Exhibit a New Secondary-Structure Motif. *Nature* **2015**, *526* (7573), 415-420. doi:10.1038/nature15363
12. Ando, T.; Uchihashi, T.; Scheuring, S., Filming Biomolecular Processes by High-Speed Atomic Force Microscopy. *Chem. Rev.* **2014**, *114* (6), 3120-3188. doi:10.1021/cr4003837
13. Rajendran, A.; Endo, M.; Sugiyama, H., State-of-the-Art High-Speed Atomic Force Microscopy for Investigation of Single-Molecular Dynamics of Proteins. *Chem. Rev.* **2014**, *114* (2), 1493-1520. doi:10.1021/cr300253x
14. Chen, J.; Zhu, E.; Liu, J.; Zhang, S.; Lin, Z.; Duan, X.; Heinz, H.; Huang, Y.; De Yoreo, J. J., Building Two-Dimensional Materials One Row at a Time: Avoiding the Nucleation Barrier. *Science* **2018**, *362* (6419), 1135. doi:10.1126/science.aau4146
15. Ou, Z.; Wang, Z.; Luo, B.; Luijten, E.; Chen, Q., Kinetic Pathways of Crystallization at the Nanoscale. *Nature Materials* **2020**, *19* (4), 450-455. doi:10.1038/s41563-019-0514-1
16. Tan, S. F.; Chee, S. W.; Lin, G.; Mirsaidov, U., Direct Observation of Interactions between Nanoparticles and Nanoparticle Self-Assembly in Solution. *Accounts of Chemical Research* **2017**, *50* (6), 1303-1312. doi:10.1021/acs.accounts.7b00063

17. Song, M.; Zhou, G.; Lu, N.; Lee, J.; Nakouzi, E.; Wang, H.; Li, D., Oriented Attachment Induces Fivefold Twins by Forming and Decomposing High-Energy Grain Boundaries. *Science* **2020**, *367* (6473), 40. doi:10.1126/science.aax6511
18. De wael, A.; De Backer, A.; Jones, L.; Varambhia, A.; Nellist, P. D.; Van Aert, S., Measuring Dynamic Structural Changes of Nanoparticles at the Atomic Scale Using Scanning Transmission Electron Microscopy. *Physical Review Letters* **2020**, *124* (10), 106105. doi:10.1103/PhysRevLett.124.106105
19. Chamberlain, T. W.; Biskupek, J.; Skowron, S. T.; Markevich, A. V.; Kurasch, S.; Reimer, O.; Walker, K. E.; Rance, G. A.; Feng, X. L.; Mullen, K.; Turchanin, A.; Lebedeva, M. A.; Majouga, A. G.; Nenajdenko, V. G.; Kaiser, U.; Besley, E.; Khlobystov, A. N., Stop-Frame Filming and Discovery of Reactions at the Single-Molecule Level by Transmission Electron Microscopy. *Acs Nano* **2017**, *11* (3), 2509-2520. doi:10.1021/acsnano.6b08228
20. Maksov, A.; Dyck, O.; Wang, K.; Xiao, K.; Geohegan, D. B.; Sumpter, B. G.; Vasudevan, R. K.; Jesse, S.; Kalinin, S. V.; Ziatdinov, M., Deep Learning Analysis of Defect and Phase Evolution during Electron Beam-Induced Transformations in WS₂. *npj Comput. Mater.* **2019**, *5*, 8. doi:10.1038/s41524-019-0152-9
21. Pennycook, T. J.; Jones, L.; Pettersson, H.; Coelho, J.; Canavan, M.; Mendoza-Sanchez, B.; Nicolosi, V.; Nellist, P. D., Atomic Scale Dynamics of a Solid State Chemical Reaction Directly Determined by Annular Dark-Field Electron Microscopy. *Scientific Reports* **2014**, *4*. doi:7555
10.1038/srep07555
22. Mishra, R.; Ishikawa, R.; Lupini, A. R.; Pennycook, S. J., Single-Atom Dynamics in Scanning Transmission Electron Microscopy. *MRS Bull.* **2017**, *42* (9), 644-652. doi:10.1557/mrs.2017.187
23. Wittkowski, R.; Tiribocchi, A.; Stenhammar, J.; Allen, R. J.; Marenduzzo, D.; Cates, M. E., Scalar Phi(4) Field Theory for Active-Particle Phase Separation. *Nature Communications* **2014**, *5*, 9. doi:10.1038/ncomms5351
24. Knobler, C. M.; Desai, R. C., Phase-Transitions in Monolayers. *Annu. Rev. Phys. Chem.* **1992**, *43*, 207-236. doi:10.1146/annurev.pc.43.100192.001231
25. Zahn, K.; Maret, G., Dynamic Criteria for Melting in Two Dimensions. *Physical Review Letters* **2000**, *85* (17), 3656-3659. doi:10.1103/PhysRevLett.85.3656
26. Boattini, E.; Dijkstra, M.; Filion, L., Unsupervised Learning for Local Structure Detection in Colloidal Systems. *J. Chem. Phys.* **2019**, *151* (15), 12. doi:10.1063/1.5118867
27. Long, A. W.; Ferguson, A. L., Nonlinear Machine Learning of Patchy Colloid Self-Assembly Pathways and Mechanisms. *J. Phys. Chem. B* **2014**, *118* (15), 4228-4244. doi:10.1021/jp500350b
28. Cichos, F.; Gustavsson, K.; Mehlig, B.; Volpe, G., Machine Learning for Active Matter. *Nat. Mach. Intell.* **2020**, *2* (2), 94-103. doi:10.1038/s42256-020-0146-9
29. Reinhart, W. F.; Long, A. W.; Howard, M. P.; Ferguson, A. L.; Panagiotopoulos, A. Z., Machine Learning for Autonomous Crystal Structure Identification. *Soft Matter* **2017**, *13* (27), 4733-4745. doi:10.1039/c7sm00957g
30. Xie, T.; Grossman, J. C., Crystal Graph Convolutional Neural Networks for an Accurate and Interpretable Prediction of Material Properties. *Physical Review Letters* **2018**, *120* (14), 145301. doi:10.1103/PhysRevLett.120.145301
31. Xie, T.; France-Lanord, A.; Wang, Y.; Shao-Horn, Y.; Grossman, J. C., Graph Dynamical Networks for Unsupervised Learning of Atomic Scale Dynamics in Materials. *Nature Communications* **2019**, *10* (1), 2667. doi:10.1038/s41467-019-10663-6
32. Wang, J.; Ferguson, A. L., Nonlinear Machine Learning in Simulations of Soft and Biological Materials. *Mol. Simul.* **2018**, *44* (13-14), 1090-1107. doi:10.1080/08927022.2017.1400164

33. Grazioli, G.; Martin, R. W.; Butts, C. T., Comparative Exploratory Analysis of Intrinsically Disordered Protein Dynamics Using Machine Learning and Network Analytic Methods. *Front. Mol. Biosci.* **2019**, *6*, 20. doi:10.3389/fmolb.2019.00042
34. Wehmeyer, C.; Noe, F., Time-Lagged Autoencoders: Deep Learning of Slow Collective Variables for Molecular Kinetics. *J. Chem. Phys.* **2018**, *148* (24), 9. doi:10.1063/1.5011399
35. Adorf, C. S.; Moore, T. C.; Melle, Y. J. U.; Glotzer, S. C., Analysis of Self-Assembly Pathways with Unsupervised Machine Learning Algorithms. *J. Phys. Chem. B* **2020**, *124* (1), 69-78. doi:10.1021/acs.jpcc.9b09621
36. Narayan, V.; Menon, N.; Ramaswamy, S., Nonequilibrium Steady States in a Vibrated-Rod Monolayer: Tetratic, Nematic, and Smectic Correlations. *J. Stat. Mech.-Theory Exp.* **2006**, *17*, P01005. doi:10.1088/1742-5468/2006/01/p01005
37. Jiao, Y.; Stillinger, F. H.; Torquato, S., Distinctive Features Arising in Maximally Random Jammed Packings of Superballs. *Physical Review E* **2010**, *81* (4), 8. doi:10.1103/PhysRevE.81.041304
38. Kingma, D. P.; Welling, M., Auto-Encoding Variational Bayes. **2013**, *arXiv:1312.6114*. *arXiv.org e-Print archive*. <https://arxiv.org/abs/1312.6114>,
39. Kingma, D. P.; Welling, M., An Introduction to Variational Autoencoders. *Foundations and Trends® in Machine Learning* **2019**, *12* (4), 307-392. doi:10.1561/22000000056
40. Doersch, C., Tutorial on Variational Autoencoders. **2021**, *arXiv:1606.05908*. *arXiv.org e-Print archive*. <https://arxiv.org/abs/1606.05908>,
41. Yamada, T.; Hosoe, M.; Kato, K.; Yamamoto, K. The Character Generation in Handwriting Feature Extraction Using Variational Autoencoder. In *Proceedings of the 14th IAPR International Conference on Document Analysis and Recognition (ICDAR)*, Kyoto, Japan, 2017, pp. 1019-1024, doi: 10.1109/ICDAR.2017.169.
42. Linh Tran, D.; Walecki, R.; Eleftheriadis, S.; Schuller, B.; Pantic, M. DeepCoder: Semi-Parametric Variational Autoencoders for Automatic Facial Action Coding. In *Proceedings of the 2017 IEEE International Conference on Computer Vision (ICCV)*, Venice, Italy, 2017, pp. 3209-3218, doi: 10.1109/ICCV.2017.346.
43. Pyles, H.; Zhang, S.; De Yoreo, J. J.; Baker, D., Controlling Protein Assembly on Inorganic Crystals through Designed Protein Interfaces. *Nature* **2019**, *571* (7764), 251-256. doi:10.1038/s41586-019-1361-6
44. Ziatdinov, M.; Dyck, O.; Maksov, A.; Li, X. F.; San, X. H.; Xiao, K.; Unocic, R. R.; Vasudevan, R.; Jesse, S.; Kalinin, S. V., Deep Learning of Atomically Resolved Scanning Transmission Electron Microscopy Images: Chemical Identification and Tracking Local Transformations. *ACS Nano* **2017**, *11* (12), 12742-12752. doi:10.1021/acsnano.7b07504
45. Wang, F.; Eljarrat, A.; Müller, J.; Henninen, T. R.; Erni, R.; Koch, C. T., Multi-Resolution Convolutional Neural Networks for Inverse Problems. *Scientific Reports* **2020**, *10* (1), 5730. doi:10.1038/s41598-020-62484-z
46. Ziatdinov, M.; Maksov, A.; Kalinin, S. V., Learning Surface Molecular Structures *via* Machine Vision. *npj Comput. Mater.* **2017**, *3*, 31. doi:10.1038/s41524-017-0038-7
47. Oztel, I.; Yolcu, G.; Ersoy, I.; White, T.; Bunyak, F. Mitochondria Segmentation in Electron Microscopy Volumes Using Deep Convolutional Neural Network. In *Proceedings of 2017 IEEE International Conference on Bioinformatics and Biomedicine (BIBM)*, Kansas City, MO, USA, 2017, pp. 1195-1200, doi: 10.1109/BIBM.2017.8217827.
48. Modarres, M. H.; Aversa, R.; Cozzini, S.; Ciancio, R.; Leto, A.; Brandino, G. P., Neural Network for Nanoscience Scanning Electron Microscope Image Recognition. *Scientific Reports* **2017**, *7* (1), 13282. doi:10.1038/s41598-017-13565-z

49. Ezzat, D.; Taha, M. H. N.; Hassanien, A. E. An Optimized Deep Convolutional Neural Network to Identify Nanoscience Scanning Electron Microscope Images Using Social Ski Driver Algorithm. In Proceedings of the International Conference on Advanced Intelligent Systems and Informatics 2019, Cairo, Egypt, 2019; Hassanien, A. E.; Shaalan, K.; Tolba, M. F., Eds.; Springer International Publishing: Cham, 2020; pp 492-501. doi: 10.1007/978-3-030-31129-2_45
50. Zaimi, A.; Wabartha, M.; Herman, V.; Antonsanti, P.-L.; Perone, C. S.; Cohen-Adad, J., Axondeepseg: Automatic Axon and Myelin Segmentation from Microscopy Data Using Convolutional Neural Networks. *Scientific Reports* **2018**, *8* (1), 3816. doi:10.1038/s41598-018-22181-4
51. Konishi, K.; Mimura, M.; Nonaka, T.; Sase, I.; Nishioka, H.; Suga, M., Practical Method of Cell Segmentation in Electron Microscope Image Stack Using Deep Convolutional Neural Network. *Microscopy* **2019**, *68* (4), 338-341. doi:10.1093/jmicro/dfz016 %J Microscopy
52. Roels, J.; Vylder, J. D.; Aelterman, J.; Saeys, Y.; Philips, W. Convolutional Neural Network Pruning to Accelerate Membrane Segmentation in Electron Microscopy, In *Proceedings of the IEEE 14th International Symposium on Biomedical Imaging (ISBI 2017)*, Melbourne, VIC, Australia, 2017, pp. 633-637, doi: 10.1109/ISBI.2017.7950600.
53. Ito, E.; Sato, T.; Sano, D.; Utagawa, E.; Kato, T., Virus Particle Detection by Convolutional Neural Network in Transmission Electron Microscopy Images. *Food and Environmental Virology* **2018**, *10* (2), 201-208. doi:10.1007/s12560-018-9335-7
54. Ciresan, D.; Giusti, A.; Gambardella, L.; Schmidhuber, J. J. A. i. n. i. p. s., Deep Neural Networks Segment Neuronal Membranes in Electron Microscopy Images. **2012**, *25*, 2843-2851
55. Li, R.; Si, D.; Zeng, T.; Ji, S.; He, J. Deep Convolutional Neural Networks for Detecting Secondary Structures in Protein Density Maps from Cryo-Electron Microscopy. In *Proceedings of 2016 IEEE International Conference on Bioinformatics and Biomedicine (BIBM)*, Shenzhen, China, 2016, pp. 41-46, doi: 10.1109/BIBM.2016.7822490.
56. Zhu, Y.; Ouyang, Q.; Mao, Y., A Deep Convolutional Neural Network Approach to Single-Particle Recognition in Cryo-Electron Microscopy. *BMC Bioinformatics* **2017**, *18* (1), 348. doi:10.1186/s12859-017-1757-y
57. Rashidi, M.; Wolkow, R. A., Autonomous Scanning Probe Microscopy *in Situ* Tip Conditioning through Machine Learning. *ACS Nano* **2018**, *12* (6), 5185-5189. doi:10.1021/acsnano.8b02208
58. Ziatdinov, M.; Zhang, S.; Dollar, O.; Pfaendtner, J.; Mundy, C. J.; Li, X.; Pyles, H.; Baker, D.; De Yoreo, J. J.; Kalinin, S. V., Quantifying the Dynamics of Protein Self-Organization Using Deep Learning Analysis of Atomic Force Microscopy Data. *Nano Letters* **2021**, *21* (1), 158-165. doi:10.1021/acs.nanolett.0c03447
59. Liu, Y.; Sun, Q.; Lu, W.; Wang, H.; Sun, Y.; Wang, Z.; Lu, X.; Zeng, K., General Resolution Enhancement Method in Atomic Force Microscopy Using Deep Learning. **2019**, *2* (2), 1800137. doi:https://doi.org/10.1002/adts.201800137
60. Newby, J. M.; Schaefer, A. M.; Lee, P. T.; Forest, M. G.; Lai, S. K., Convolutional Neural Networks Automate Detection for Tracking of Submicron-Scale Particles in 2D and 3D. **2018**, *115* (36), 9026-9031. doi:10.1073/pnas.1804420115 %J Proceedings of the National Academy of Sciences
61. Rivenson, Y.; Göröcs, Z.; Günaydin, H.; Zhang, Y.; Wang, H.; Ozcan, A., Deep Learning Microscopy. *Optica* **2017**, *4* (11), 1437-1443. doi:10.1364/OPTICA.4.001437
62. Iglesias, J. C. Á.; Santos, R. B. M.; Paciornik, S., Deep Learning Discrimination of Quartz and Resin in Optical Microscopy Images of Minerals. *Minerals Engineering* **2019**, *138*, 79-85. doi:https://doi.org/10.1016/j.mineng.2019.04.032
63. Hay, E. A.; Parthasarathy, R., Performance of Convolutional Neural Networks for Identification of Bacteria in 3D Microscopy Datasets. *PLOS Computational Biology* **2018**, *14* (12), e1006628. doi:10.1371/journal.pcbi.1006628

64. Shashank Kaira, C.; Yang, X.; De Andrade, V.; De Carlo, F.; Scullin, W.; Gursoy, D.; Chawla, N., Automated Correlative Segmentation of Large Transmission X-Ray Microscopy (Txm) Tomograms Using Deep Learning. *Materials Characterization* **2018**, *142*, 203-210.
doi:<https://doi.org/10.1016/j.matchar.2018.05.053>
65. Huang, Y.; Wang, S.; Guan, Y.; Maier, A., Limited Angle Tomography for Transmission X-Ray Microscopy Using Deep Learning. *Journal of Synchrotron Radiation* **2020**, *27* (2), 477-485.
doi:[doi:10.1107/S160057752000017X](https://doi.org/10.1107/S160057752000017X)
66. Ronneberger, O.; Fischer, P.; Brox, T., U-Net: Convolutional Networks for Biomedical Image Segmentation. In *Proceedings of Medical Image Computing and Computer-Assisted Intervention (MICCAI) 2015*, Munich, Germany, 2015; Navab N., Hornegger J., Wells W., Frangi A., Eds.; Springer International Publishing: Cham, 2015, vol 9351, pp 234-241. doi:10.1007/978-3-319-24574-4_28
67. Zeng, Y.; Chen, X.; Zhang, Y.; Bai, L.; Han, J. Dense-U-Net: Densely Connected Convolutional Network for Semantic Segmentation with a Small Number of Samples, In *Proceedings of Tenth International Conference on Graphics and Image Processing (ICGIP 2018)*, Chengdu, China, 2018. p. 110692B. doi: 10.1117/12.2524406.
68. Zhou, Z.; Siddiquee, M. M. R.; Tajbakhsh, N.; Liang, J. J. D. L. i. M. I. A.; Multimodal Learning for Clinical Decision Support : 4th International Workshop, D.; 8th International Workshop, M.-C., held in conjunction with MICCAI , Granada, Spain, S... Unet++: A Nested U-Net Architecture for Medical Image Segmentation. **2018**, *11045*, 3-11
69. Xiao, X.; Lian, S.; Luo, Z.; Li, S. Weighted Res-Unet for High-Quality Retina Vessel Segmentation. In *Proceedings of 9th International Conference on Information Technology in Medicine and Education (ITME)*, Hangzhou, China, 2018, pp. 327-331, doi: 10.1109/ITME.2018.00080.
70. Lakshminarayanan, B.; Pritzel, A.; Blundell, C., Simple and Scalable Predictive Uncertainty Estimation Using Deep Ensembles. In *Proceedings of the 31st International Conference on Neural Information Processing Systems*, Curran Associates Inc.: Long Beach, California, USA, 2017; pp 6405–6416.
71. Bepler, T.; Zhong, E.; Kelley, K.; Brignole, E.; Berger, B., Explicitly Disentangling Image Content from Translation and Rotation with Spatial-Vae. *Advances in Neural Information Processing Systems* **2019**, 15409-15419
72. Bengio, Y.; Courville, A.; Vincent, P., Representation Learning: A Review and New Perspectives. *IEEE Transactions on Pattern Analysis and Machine Intelligence* **2013**, *35* (8), 1798-1828.
doi:10.1109/TPAMI.2013.50
73. Higgins, I.; Amos, D.; Pfau, D.; Racaniere, S.; Matthey, L.; Rezende, D.; Lerchner, A., Towards a Definition of Disentangled Representations. **2018**, *arXiv:1812.02230*. *arXiv.org e-Print archive*.
<https://arxiv.org/abs/1812.02230>,
74. Kingma, D. P.; Ba, J., Adam: A Method for Stochastic Optimization. 2015, *arXiv:1412.6980*.
arXiv.org e-Print archive. <https://arxiv.org/abs/1412.6980>,
75. Ziatdinov, M., Atomai. In *GitHub repository*, <https://github.com/pycroscopy/atomai>, 2020.

TOC

